Partially pyrolyzed-non-activated olive stones: Characterization and utilization of olive stones partially-pyrolyzed at various temperatures for 2-chlorophenol removal from water

El-Sheikh, A. H. & Newman, A

DOI 10.1016/j.emcon.2023.100209
ISSN 2405-6650
ESSN 2405-6642

Publisher: Elsevier

Emerging Contaminants 9 (2023) 100209

Contents lists available at ScienceDirect

Emerging Contaminants

journal homepage: www.keaipublishing.com/cn/journals/emerging-contaminants

Partially pyrolyzed-non-activated olive stones: Characterization and utilization of olive stones partially-pyrolyzed at various temperatures for 2-chlorophenol removal from water

Amjad H. El-Sheikh [a, *], Alan P. Newman [b]

[a] Department of Chemistry, Faculty of Science, The Hashemite University, P.O. Box 330127, Zarqa, 13133, Jordan
[b] Centre for Agroecology Water and Resilience (CAWR), Coventry University, Wolston Lane, Ryton on Dunsmore, CV8 3LG, UK

ARTICLE INFO

Article history:
Received 21 December 2022
Received in revised form
16 January 2023
Accepted 25 January 2023
Available online 27 January 2023

Keywords:
Olive stones
Controlled pyrolysis
Water treatment
Adsorption of phenols

ABSTRACT

This paper reports the development of the chemical and structural properties of partially pyrolyzed olive stones (OS) (at 250, 400, 500, 600, 700 and 850 °C) intended for use as a less expensive and more environmental-friendly adsorbent within water treatment applications. The following properties were followed: mass loss, surface chemistry (acid/base titrations and IR analysis), crystalline matter and elemental analysis, SEM, BET and TGA analysis. The major mass loss (68%) occurred between 250 and 400 °C. Acidic oxides disappeared after 500 °C, while surface basicity increased with increasing pyrolysis temperature. The partially pyrolyzed-non-activated OS sorbents were used for 2-chlorohenol (2-CP) removal from water, where 2-CP uptake increased with increasing pyrolysis temperature. The maximum adsorption was recorded at pH 7 using the pyrolyzed OS at 850 °C, which was only 13% more than that of OS pyrolyzed at 600 °C (sorbent carb600). So that carb600 (adsorption capacity: 34.1 mg g^{-1}) was recommended as a cost-effective-environmental-friendly adsorbent. The re-usability of carb600 for removing 2-chlorophenol from real water sample was evident, where ~70% of its adsorption efficiency was reserved even in the presence of competing ions.

1. Introduction

Adsorption has proven itself as a powerful method for water treatment, especially when the contaminants of interest are at low concentration. There is a continuous effort to prepare efficient, environmental-friendly and inexpensive adsorbents. Activated carbon has been widely used for both pollution control and potable water treatment [1–4]. Reports have appeared on the preparation of activated carbons with adequate adsorptive properties from various agricultural biomass by-products [4–10]. However, preparation of activated carbon is a costly process and cause the emission of greenhouse gases both in the initial pyrolysis step and, in many instances, in a subsequent activation step using superheated steam. In response, the use of raw agricultural by-products (such as fruit stones) was suggested as alternative environmental-friendly cheap bio-sorbents [11–24]. The use of olive-based biomass sorbents has been used for water treatment [25–29]. However, there remains a need for physical and chemical treatment of these adsorbents to improve their properties. This has included deposition of magnetite to improve their physical separation from the adsorption medium [4,30–33], solvent treatment to remove soluble matter [34] and heat treatment [26,34,35]; in addition to other modification methods [36]. It is suggested in the present work to undertake partial pyrolysis of the lignocellulosic material (within the range 250–700 °C), which may be an alternative process to complete carbonisation at 850 °C and omitting the steam activation step. This consumes less energy, and potentially gives more adsorbent mass with less gas emissions. A less technically demanding process also encourages the pyrolysis taking place close to the source of feedstock.

Pyrolysis of olive stones was previously investigated by groups in Spain and Greece [37,38], in which various carbons were produced under various heating rates, carbonisation temperatures, residence times, activating agents, furnace type, etc. Recent studies

* Corresponding author.
E-mail addresses: amjadelsheikh3@yahoo.com, elsheikh@hu.edu.jo (A.H. El-Sheikh).
Peer review under responsibility of KeAi Communications Co., Ltd.

https://doi.org/10.1016/j.emcon.2023.100209

reported the use of pyrolyzed olive stones for treatment of metal ions [6,17,39,40], organic dyes; nitrate [7,41], phenolic compounds [5], pharmaceutical wastewater [42], olive mill wastewater [4], enzymes [43]. Different olive varieties have different properties of oil content, texture, density, composition of lignocellulosic material and inorganic content, which may all affect the carbonisation process [25]. Thus the olive composition and subsequent carbon properties is certainly dependent on the variety and on the soil conditions in which the olives are cultivated.

Previous works that involved carbon preparation usually selected 850 °C as a temperature for carbonisation as a literature value because many authors reported it as an optimum temperature for both carbonisation and activation of olive stones and some other precursors [44]. However, the critical question is whether this temperature is the optimum for the type of feedstock used, and what is expected to happen if lower temperatures are used?

In the present work, the specific chemical, structural and adsorption properties of Jordanian olive stones (variety *Nabali*) have been studied. None of the previous studies reported this issue. So that samples of ground and dried olive stones were partially carbonised at various temperatures, i.e. 110-850 °C. Each partially pyrolyzed sorbent was studied in terms of mass lost upon pyrolysis, ultimate-elemental-analysis, presence of crystalline matter, surface chemistry, surface morphology and porosity, and surface acidity/basicity. Pyrolysis of olive stones was also studied by thermal gravimetric analysis (TGA) at various heating rates. Adsorption of 2-chlorophenol (2-CP) using the prepared pyrolyzed samples was investigated to explore the effect of pyrolysis temperature on adsorption behaviour.

2-CP was selected in the present work as model pollutant to test the efficiency of the partially pyrolyzed-non-activated olive stones. 2-CP has wide industrial applications and it has high solubility in water. Phenols may be produced from pesticides degradation and from natural and industrial processes [45,46]. They occur widely in industrial effluents such as those from refineries and coal tar distillation, plastic, paint, pharmaceutical industries, paper industries and steel industries. Chlorophenols are generally believed to be of great concern as potential pollutants. They are highly toxic, hematotoxic, hepatotoxic, potentially carcinogenic and in general not-easily biodegradable [45–50]. From the water industry's point of view, they also have extremely low odour and taste thresholds. Many chlorinated phenols were listed as US-priority pollutants. The continuously increasing amount of agricultural and industrial wastewater may cause severe problems. So that there is a continuous need to develop efficient and costly-effective water treatment methods for pollutants removal.

2. Experimental

2.1. Materials

The olives used in the present work (variety *Nabaly*) were grown near to Amman city (Jordan) and were purchased from a local market. The olive fruit was removed and the remaining olive stones were dried at 110 °C for 24 h before use. 2-Chlorophenol (**2-CP**) was purchased from Fluka (Italy).

2.2. Partial pyrolysis of olive stones

For the purpose of following the carbonisation process of olive stones and the development of textural and chemical properties, 15 g samples of olive stones were crushed using a hammer and ground using a Micro Hammer Cutter Mill, fitted with a 3 mm screen. The milled material was then weighed, dried at 110 °C overnight and re-weighed. This was labelled as ground dried olive stones (**carb110**). Pyrolysis then took place for each sample, separately, at 250, 400, 500, 600, 700 and 850 °C in a horizontal tube furnace (Lenton Thermal Design LTD) fitted with a Eurotherm temperature controller, under nitrogen gas atmosphere (flow rate 3.0 L min^{-1}). The heating rate, starting from room temperature, was 200 °C/min. The furnace was programmed to keep the final temperature for 2 h, in which the pyrolysis process continued during this period. The furnace was then switched off and the sample was left to cool inside the tube furnace for 3 h under a nitrogen gas atmosphere (flow rate was reduced to 300 mL/min to reduce mass loss), after which the mass of partial carbonisation was estimated. Mass loss was estimated relative to carb250. Samples were labelled based on the temperature of pyrolysis and are thus listed as: **carb110** (ground olive stones-dried at 110 °C), **carb250**, **carb400**, **carb500**, **carb600**, **carb700** and **carb850**. For comparison purposes and to study the effect of steam activation: a sample of carb850 was activated by steam as described in a previous work [44] and the product was labelled as **carb850-activated**.

2.3. Characterization of the ground dried olive stones (carb110) and the partially pyrolyzed olive stones

The approximate analysis of the ground dried olive stones (carb110) was carried out following the methods described by Sjostrom [51], so as to determine cellulose, hemicellulose and lignin contents. Thermal gravimetric analysis (TGA) of ground dried olive stones (carb110) was carried out by using a Setaram TGA 92−12 instrument starting from room temperature up to 850 °C under nitrogen atmosphere with various heating rates employed, i.e. 20, 50 and 100 °C/min.

Powder x-ray diffraction patterns were obtained using a Phillips x-ray diffractometer PW1700, with copper tube. Infrared spectra were measured as KBr disks on a Nicolet 210 Fourier-transform infrared spectrometer. Scanning electron micrographs (SEM) were obtained, without sample coating, using a JEOL JSM-5600LV scanning electron microscope. Carbon, hydrogen and nitrogen (CHN) were analysed by an Exeter Analytical Model CE440, and oxygen content was estimated by the difference between the total content and the sum of the CHN and ash content. Nitrogen (N_2) adsorption experiments were conducted at 77 K to measure the BET specific surface area (SA_{BET}) using an OMNISORB 360 nitrogen porosimeter.

Ash content was estimated by dry ashing. Samples (1.0 g each) were placed in a pre-weighed crucible. Each sample was heated in a high temperature furnace (Lenton Thermal Design LTD, Eurotherm temperature controller) at 650 °C for 24 h in an air atmosphere. The final mass was measured and the percentage ash content was calculated. The ash obtained from ground dried olive stones (carb110) and carb850 was subject to analysis by inductively coupled plasma (ICP) emission spectrometer (PerkinElmer Plasma 400) after dissolution for 8 h with 25 mL of 5% HNO_3. Further semi-quantitative elemental analysis of carb110 and carb850 was conducted using Phillips x-ray fluorescence PW1410 system, fitted with a chromium tube.

Acid/base titrations analogous to Boehm titrations have been previously described [52] and have been widely used to determine acidic/basic surface oxides. Relative surface area estimation by using the methylene blue adsorption method was described in a previous work [27].

2.4. Adsorption of 2-CP from water

Adsorption of 2-CP on partially pyrolyzed OS was studied in separate experiments. 100 mg L^{-1} stock solution of 2-CP was prepared separately in 0.01 M sodium hydroxide as the solvent to ensure complete dissolution of 2-CP in aqueous medium. From this

stock solution, 25 mL of each of the following standard solutions were prepared: 20, 40, 60, 80, 90 and 100 mg L^{-1}. These solutions were added separately to conical flasks each containing 25 mg of the desired pyrolyzed OS sorbent where the desired pH of the solution was adjusted using dilute nitric acid or sodium hydroxide. The flasks were shaken for 3 h at 30 °C using isothermal water bath shaker. The supernatant was recovered using a pipette and 2-CP was analysed as previously described [44]. The following equations were then applied:

$q_e = (C_o - C_e).V/m$ Surface concentration.

$C_e/q_e = 1/K_L + (1/X_m).C_e$ Langmuir equation.

In which, C_o: initial concentration (mg L^{-1}), C_e: equilibrium concentration (mg L^{-1}), q_e: surface concentration (mg g^{-1}), V: volume of the solution (L), m: mass of adsorbent (gram), X_m: monolayer capacity (mg g^{-1}), K_L: Langmuir constant.

3. Results and discussion

The adsorption of any pollutant greatly depends on the surface properties of the carbon-based material (surface chemistry and textural properties) [53–63]. These properties depend on the biomass precursor, carbonisation conditions and impurities. So that it was intended in the present work to study the properties of OS (section 3.1) and the progress of partially pyrolyzed OS at various temperatures (section 3.2) prior to its use in 2-CP removal from water (section 3.3).

3.1. Chemical and structural properties of olive stones (OS)

3.1.1. Analysis of inorganic content by ICP and XRF

Elemental analysis of olive stones and carb850 by ICP and XRF are presented in Table 1. XRF results are given as peak intensities and are presented in arbitrary units for the elements, as they appeared in the XRF spectra. Relatively high amounts of alkaline metals existed, probably due to the geochemistry of the soils in the region from which the olives were obtained. Low amounts heavy metals (Fe, Zn, Cu, As, Pb, Ni, Cr) were also observed in olive stones. Because of the decrease in mass due to carbonisation, these were significantly concentrated in carb850 to different extents (enrichment factors are given in Table 1). Relatively large sulphur and chlorine amounts appeared in the olive stones, but decreased in carb850, presumably due to high temperature treatment of the sample. The opposite was for phosphorus and strontium. Small peaks for aluminium and silicon were detected. The presence of this mixture of elements may give an indication as to the possible presence of crystalline compounds, which may affect the behaviour of the pyrolyzed samples. The presence of ash had a negative impact on the adsorption properties due to its contribution to the weight of the sample [64]. However, de-mineralization, i.e. de-ashing, is usually carried out by using strong chemicals, which may be responsible for negative textural and structural changes in the samples [64].

3.1.2. Approximate analysis

The organic constituents have a potential effect on the pyrolysis process and thus both the mineral content and organic constituents are important preliminary parameters that should be quantified in any study on carbon. The chemical constituents in olive stones are presented in Table 1. The high percentage of lignin explains the hardness of olive stones. For comparative purposes, Overend and Chornet [65] reported that olive stones from Spain gave 8 % wt moisture, 0.3 % wt ether extract, 4.7 % wt alcohol-benzene extract, 31.2 % wt lignin, 34.6 % wt hollocellulose and 10.1 % wt α-cellulose. Knowledge of these components was important when gravimetric decomposition behaviour of olive stones was studied (see section 3.1.4).

Table 1
Chemical composition of ground dried OS (carb110) and carb850.

	Carb110	Carb850	
ICP analysis	**mg metal . Kg^{-1}**	**mg metal . Kg^{-1}**	**Enrichment factor**
Ca	1550	5120	3.3
K	1025	3750	3.7
Mg	365	1920	5.2
Na	119	750	6.3
Fe	13.5	47.5	3.5
Zn	10.3	27.5	2.7
Cu	4.8	4.6	0.9
As	0.5	1.1	2.2
Pb	0.4	1.2	3.0
Ni	0.5	2.2	4.4
Cr	0.1	0.4	4.4
XRF analysis	**Peak intensity (x 10^2)**	**Peak intensity (x 10^2)**	**Enrichment factor**
Al	0.6	1.2	2.0
Si	11	24.5	2.2
P	95	1070	11.3
S	162	80.5	0.5
Cl	39	11.5	0.3
Mn	5.0	16.6	3.3
Sr	65	215.5	3.3
Approximate analysis	wt%		
Moisture	7.90	–	–
Ether extrac	4.85	–	–
Alcohol extract	4.95	–	–
Holocellulose	39.0	–	–
Hemicellulose	21.6	–	–
α-Cellulose	17.4	–	–
Lignin	39.6	–	–
Recover	88.6	–	–

3.1.3. FT-IR analysis

The major components of olive stones (more than 78% by mass) are cellulose, hemicellulose and lignin. Functional groups related to these compounds should be predominant in the IR spectrum of olive stones. From the literature, it is known that the functional groups that are present in cellulose are: O-, CH_2−OH, CH−OH; in softwood hemicellulose: O-, CH_2−OH, CH−OH; in hardwood hemicellulose: O-, CH_2−OH, CH−OH and −COOH; in lignin: benzene ring, ph-O-R, HO-ph-O-CH_3, aldehyde group, ph−C(O)−R, ph-C(H)(R)-OH, −C═C-ph. However, additional peaks may arise due to chemical reactions between various functional groups related to various constituents. Acid/base (Boehm) titrations (Table 2) showed that ground dried olive stones (carb110) did not show any π-basicity, due to absence of graphene sheets. Acidic groups (carboxylic, lactonic and phenolic) were present in the order: lactonic > carboxylic > phenolic.

The infrared absorption peaks of ground dried olive stones (carb110) along with their assignments, are shown in Table 3. The absorption peaks of olive stones were classified according to their correspondence to a single functional group. So that:

- Two absorption bands were assigned to various vibrational modes of hydroxyl group, i.e. O−H stretching and O−H in-plane bending.
- Many aliphatic C−H vibrations were identified, i.e. C−H asymmetrical stretching, C−H symmetrical stretching, CH_3 asymmetrical bending which overlaps with scissoring CH_2, CH_3 symmetrical bending, CH_2 wagging and twisting, CH_2 rocking, C−C stretching and C−C bending.
- Carbonyl group was assigned to an aldehyde group or aliphatic ester.
- Many peaks were assigned to alkenes and aromatics, i.e. C−C stretching in mononuclear aromatic, ring C−H out of plane bending, C═C stretching of unsymmetrical diene.
- Three peaks were assigned to etheric groups, i.e. asymmetrical stretching in alkyl-aryl ether, asymmetrical stretching in aliphatic ether, symmetrical stretching in alkyl-aryl ether.
- Two peaks were related to alcohol, i.e. C−O stretching and O−H stretching.

Some IR absorption peaks that may be used to follow the major components of olive stones during pyrolysis are: for lignin, the peak at 1739 cm^{-1} due to C═O stretching, the peak at 1604 cm^{-1} due to unsymmetrical diene, and the peak at 1508 cm^{-1} due to benzene. For hemicellulose and cellulose: the peak at 1161 cm^{-1} is due to antisymmetrical bridge stretching, the peak at 1048 cm^{-1} is due to C−O stretching.

3.1.4. Thermal gravimetric analysis (TGA) of ground dried olive stones (carb110)

TGA results for carb110 at various heating rates, presented as percentage weight loss, and its first derivative (DTg) are shown in Fig. 1. It was noted that the generation of gas initiated at low temperature: 200, 250 and 300 °C, for the corresponding heating rates 20, 50, 100 °C/min, respectively. Each run showed, in the DTg, two peaks: at 20 °C/min: the spikes appeared at 280 °C and 360 °C; at 50 °C/min: the spikes appeared at 330 °C and 390 °C; at 100 °C/min: the spikes appeared at 340 °C and 400 °C.

In the TGA curves, it was noted that as heating rate increases, there was a shift in the curves to higher temperature. In the DTg curves, there were two peaks. The peak that appeared at lower temperature in the DTg of ground olive stones mainly represents hemicellulose degradation while the peak at higher temperature was related to cellulose. Lignin decomposition occurred at all temperatures but mainly at high temperatures [66].

It has been generally recognized that the TGA of wood-like material is composite of the TGA curves for hemicellulose and cellulose, knowing that isolated cellulose and hemicellulose usually decompose at lower temperatures than in the biomass itself. This was attributed to a catalytic effect of the other components in the matrix trace metals. The presence of inorganic matter (particularly sodium, potassium and calcium) affects the carbonisation process and the properties of the carbon produced [64]. This leads to lower yields of carbonisation than expected. Additionally, they may catalyze the carbonisation process and thus decrease the yield. In

Table 2
Effect of stepwise pyrolysis on partially pyrolyzed OS properties.

	Carb110	Carb250	Carb400	Carb500	Carb600	Carb700	Carb850
CHNO and ash analysis							
% C	51.3	57.0	66.7	69.5	81.2	84.9	85.5
% H	6.3	6.3	4.8	3.3	2.6	2.2	1.6
% N	0.5	1.6	1.9	1.8	1.9	1.2	1.8
% O	41.2	33.7	24.5	22.5	10.4	7.5	5.9
%ash	0.7	1.4	2.1	2.9	3.9	4.2	5.2
Surface oxides (Boehm titrations)							
Total basic groups (meq g^{-1})	0	0.05	0.12	0.22	0.40	0.40	0.57
Total acidic groups (meq g^{-1})	0.92	0.43	0.37	0.14	0	0	0
Carboxylic groups (meq g^{-1})	0.26	0.24	0.19	0.11	0	0	0
Lactonic groups (meq g^{-1})	0.52	0.14	0.14	0	0	0	0
Phenolic groups (meq g^{-1})	0.13	0.05	0.04	0.03	0	0	0
Crystalline matter (estimated by visual interpretation of the diffraction patterns using arbitrary index (range 0-6) according to peak height)							
	CaO_2 (2 units)	CaO_2 (2 units)	–	MgO (4 units)	MgO (6 units)	MgO (6 units)<	MgO + CaO (4 units) (2 units)
Surface area[a]							
S_{MB} (m^2 g^{-1})	61.5	21.2	–	–	–	–	68.7
S_{BET} (m^2 g^{-1})	3	–	–	–	179	–	349
V_{tot} (cm^3 g^{-1})	–	–	–	–	0.168	–	0.188
V_{μ} (cm^3 g^{-1})	–	–	–	–	0.135	–	0.168
Weight loss data							
Weight loss (%)[b]	0	19.8	56.0	71.2	79.0	80.5	82.4
% mass remaining[c]	100	80.2	44.0	28.8	21.0	19.5	17.6
% pyrolysis[c]	0	24.1	68.1	86.4	95.9	97.7	100

[a] S_{MB}: methylene blue relative surface area, S_{BET}: specific surface area, V_{tot}: Total pore volume, V_{μ}: micro pore volume.
[b] Relative to carb110.
[c] Relative to carb850.

Table 3
IR absorption peaks and their assignments for partially pyrolyzed OS.

	Carb110		Carb250		Carb400		Carb500		Carb600		Carb700		Carb850	
	cm^{-1}	P.H	cm^{-1}	P.H	cm^{-1}	P.H	cm^{-1}	P.H	cm^{-1}	P.H	cm^{-1}	P.H	cm^{-1}	P.H
O–H (H-bonded)														
O–H stretch	3428	23.5	3428	14	3428	4	3428	3	3445	1.8	3445	1.3	3450	1.8
In-plane bending	1422	1.5	1422	0.8	1421	0.8	1416	0.8	1416	1.0	1416	0.5	1421	0.8
H–O–H deformation of adsorbed water	1646	3.0	1618	2.5	1601	3.5	1578	2.5	1560	1.0	1560	0.2	1623	0.3
OH association band in cellulose and hemicellulose	1116	Sh	1107	1.3	1118	0.2	flat		1121	7.0	1124	0.2	1118	0.05
Aliphatic														
Asym C–H stretch	2936	10	2925	4	2924	1	2918	0.05	2918	0.1	–		–	
Sym C–H stretch	2863	4.0	2857	1.5	2857	0.3	2845	0.05	2845	0.1				
Asym CH_3 bending, which overlap with scissoring CH_2	1461	5	1455	1.3	–		–		–		–		–	
Sym CH_3 bending	1371	3.0	1370	0.8	1370	0.2	–		–		–		–	
CH_2 Wagging and Twisting	1329	1.0	1326	0.4	1315	0.2	Flat		–		–		–	
	1245	7.0	1239	1.5	1245	0.2								
CH_2 rocking	717	Sh	717	Sh	–		–		–		–		–	
C–C stretching	894	1.0	900	sh	–		–		–		–		–	
C–C bending	439	0.5	439	0.3	445	0.2	445	sh	–		–		–	
Aldehyde														
C=O stretch	1739	17	1738	6.5	–		–		–		–		–	
Un-assigned					1695	1.0	1695	0.5	–		–		–	
Alkenes and aromatics														
C–C stretch in mononuclear aromatic	1508	6.0	1508	2	1511	0.2	–		–		–		–	
Ring C–H out of plane bending	894	1.0	900	0.5	870	0.1	871	0.4	871	0.8	871	0.3	871	1.0
	827	0.5	666	0.6	817	0.1	815	0.4	813	0.3	812	0.1	681	0.05
	662	sh			755	0.3	750	0.4	748	0.1				
					675	0.5	683	0.4	681	0.1				
C=C stretch of unsym diene	1604	Sh	1618 (new) asym stretch of sym conj diene or alkene conj with aromatic ring	2.5	1601	3.5	1578	2.5	1560	1.0	1560	0.2	1623	0.3
Etheric C–O–C														
Asym stretch of alkyl-aryl ether	1245	7.0	1239	1.5	1245	0.2	flat		–		–		–	
C–O–C antisym bridge stretching vibration in cellulose and hemicellulose	1161	5.0	1160	1.3	1163	0.2	flat		–		–		–	
Sym stretch in alkyl-aryl ether	1048	16	1045	4.0	–		–		1054	sh	1055	0.2	1045	0.05

P.H: peak height by % Transmittance.

the present TGA experiments, the average rate of total mass loss was calculated from the total mass lost and total residence time, shown in Table 4. It is clear that the rate of mass loss is directly proportional to heating rate. This relationship can be used to control the carbonisation process to a degree, in which controlling the heating rate may control the rate of carbonisation loss, and thus the amount of mass loss may be controlled within a specific period of time and a specific heating rate.

The higher the heating rate of carbonisation, the higher the rate of weight loss. At 20 °C/min, total weight loss was the largest because total residence time was the longest for that sample. The work carried out by Overend and Chornet [65] reported the larger weight loss in a fast heating rate as due faster reaction of pyrolyzed surface with the evolved gases (CO_2 and H_2O vapour). At a slow heating rate, the kinetics of pyrolytic reactions is slow.

Some studies showed that heating rate during the pyrolysis step affects greatly the composition of the volatile and char properties [67]. For example, Nazzal [68] reported that with increasing heating rate, the carbon yield decreased while reactivity and iodine number increased.

3.2. Characterization of partially pyrolyzed-non-activated olive stones

3.2.1. Development of CHNO and ash content

The results of CHNO analyses and ash content of the pyrolyzed samples are presented in Table 2. It is clear that while carbon and nitrogen contents increased upon carbonisation, those of hydrogen and oxygen decreased. Nitrogen did not show a clear tendency against pyrolysis temperature. These elemental contents are generally affected by the initial content of CHNO in the raw material and on pyrolysis conditions. Ash content (Table 2) may also affect elemental content by catalysing or inhibiting elevation of gaseous products (CO_2, CO, H_2, C_2H_2, C_2H_4, C_2H_6) [65] and thus affect the degradation process. These gases may subsequently affect the atmosphere of pyrolysis and thus affect the textural properties of the product.

3.2.2. Development of surface acidity/basicity (Boehm titrations)

In terms of ultimate analysis, special attention is usually paid to oxygen because it strongly influences the chemical properties of the carbon surface by forming functional groups (acidic or basic). The development of surface acidity/basicity was investigated by acid/base (Boehm) titrations. The results of these titrations are presented in Table 2. It should not be ignored that Boehm titrations are usually employed in the characterization of carbon and/or activated carbon, having been completely carbonised, which is not the case for all our samples. Here, partially carbonised carbons may behave differently, i.e. other functional groups may react with the added reagent.

In the present work, there was a general increase in total basicity versus pyrolysis temperature while total acidity decreased versus pyrolysis temperature. This was due to primary decomposition (thermolysis) and then secondary decomposition (aromatization) which would have rearranged these groups gradually. After 500 °C, no acidic groups appeared; lactonic group disappeared after 400 °C. The rate of disappearance of lactonic groups was higher than carboxylic groups, which may be due to the ring opening of lactonic groups into free carboxylic groups, thus reducing the rate of disappearance of carboxylic groups. However, aliphatic esters

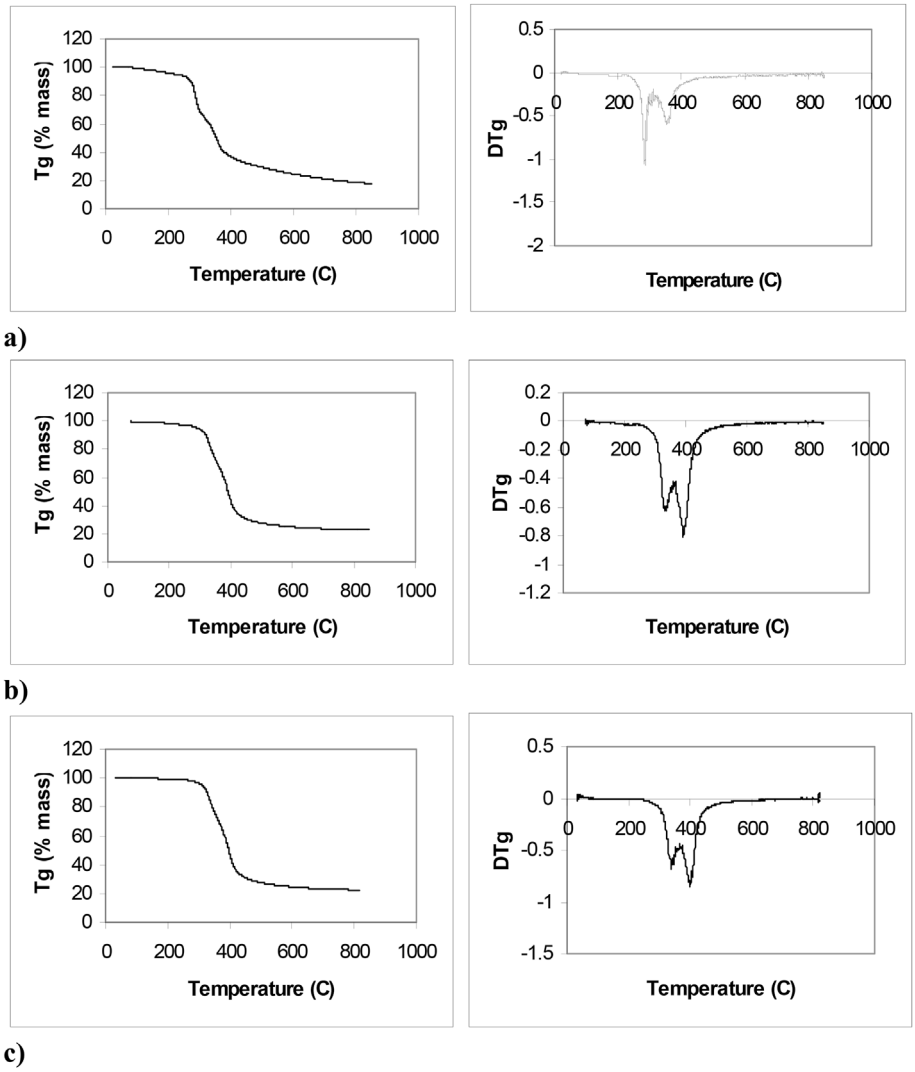

Fig. 1. TGA and DTg of ground dried OS at various heating rates: a) 20 °C/min, b) 50 °C/min and c) 100 °C/min a) fx7 b) fx8.

Table 4
TGA data for ground dried OS (carb110) at various heating rates.

Heating rate (°C min^{-1})	A = Total mass loss (%)	B = Total residence time (min)	Rate of mass loss = (A/B) (% mass loss. min^{-1})
100	77.9	8.5	9.2
50	77.5	17	4.6
20	82.5	42.5	1.9

may interfere with lactonic groups (cyclic esters) while alcoholic groups may interfere with phenolic groups. The basicity of the carbon-based sorbent is due to either pyrone-like group, or ether type group, or basicity due to π-electrons of the graphene layer [44].

3.2.3. Development of crystallographic content (XRD analysis)

The XRD analysis is presented in Table 2. It was generally noted that crystalline calcium peroxide (CaO_2), that presented in the samples up to 250 °C, has disappeared at 400 °C. However, crystalline amounts of MgO appeared at 500 °C, increased at 600 °C and remained constant until 700 °C. At 850 °C, MgO amounts decreased and calcium oxide (CaO) appeared. The presence of these minerals is possibly due to the high calcium and magnesium contents in olive stones, which may be due to high water hardness in Jordan or to the type of soil there. However, other metals such as sodium did not show any crystalline form.

3.2.4. Development of surface morphology and textural properties (SEM analysis)

Investigation of surface morphology by SEM was expected to help in following the textural properties, i.e. macroporosity, and homogeneity of the partially carbonised olive stones. The results of scanning electron microscopy (SEM) are shown in Fig. 2. Ground olive stones and carb250 did not show any pores in the SEM micrographs. Macropores appeared first in carb400. In carb500, the surface appeared to be more homogeneous and the pores were wider. In carb600, the pores became narrower than in carb500. In

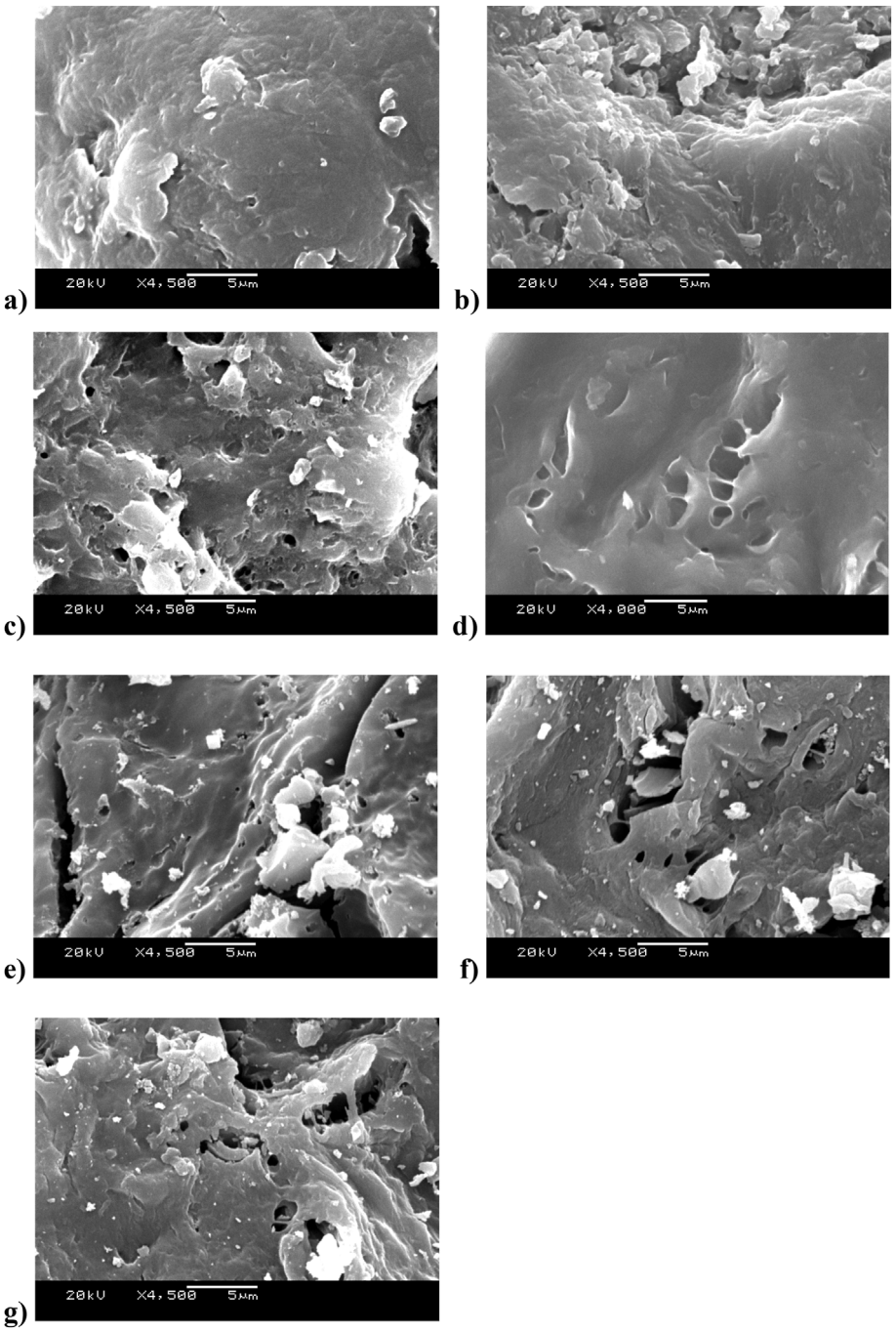

Fig. 2. SEM of a) carb110, b) carb250, c) carb400, d) carb500, e) carb600, f) carb700 and g) carb850.

carb700, wider pores appeared again with the existence of small pores. This may indicate the sequence of events of pore creation and destruction, in which small pores start, then become wider, then collapse, then new pores start again, etc.

3.2.5. Methylene blue adsorption relative surface area (S_{MB}) and BET specific surface area (S_{BET})

The results of N_2 adsorption isotherms at 77 K are shown in Fig. 3 and Table 2, from which SA_{BET} surface area were estimated as follows: carb110: 3 m^2 g^{-1}, carb600: 179 m^2 g^{-1}, carb850: 349 m^2 g^{-1}, carb850-activated: 750 m^2 g^{-1} (total pore volume: 0.425 cm^3 g^{-1}, micropore volume: 0.337 cm^3 g^{-1}). The total pore volume and micropore volume are also provided. The effect of pyrolysis temperature and steam activation on the specific surface area is very clear. It is important to mention that while SA_{BET} indicates the specific surface area based on the porosity of the adsorbent; however SA_{MB} may be more related to the surface chemistry of the adsorbent in addition to the sorbent porosity. This is in addition to the fact that methylene blue adsorption is conducted in solution and thus it is closer to real situation. The results of S_{MB} were not promising (Table 2), however, it may lead us to future work for development of new estimations for relative surface area for partially carbonised material. It may also help in indicating the nature and the behaviour of the partially carbonised material. MB

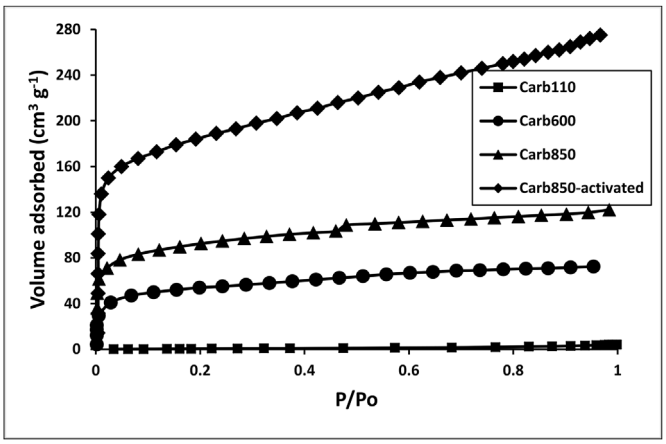

Fig. 3. N_2 adsorption onto OS-based sorbents at 77 K for BET analysis. A) fx15.

adsorption on the partially carbonised olive stones did not show easily explained results. Samples carbonised at 400, 500, 600 and 700 °C did not obey the Langmuir adsorption isotherm. This may be due to presence of tarry material and other partial degradation products of lignocellulosic material, which may partially dissolve in aqueous medium and disturb the adsorption of MB. When pyrolysis starts, many reactions start taking place. Ground olive stones exhibited MB adsorption surface area value near to that of carb850, while carb250 obeyed the Langmuir adsorption isotherm but exhibited much lower relative surface area than ground olive stones. This may be due to de-polymerisation of the polymeric lignocellulosic material.

3.2.6. Weight loss and percent yield of carbonisation

The results of weight lost and percentage yield after the partial pyrolysis of olive stones at various temperatures are presented in Table 2. The largest mass loss was between 250 and 400 °C in which primary decomposition and thermolysis of the lignocellulosic material occurred [69]. This agrees with the results in section 3.1.4, which indicate loss of nearly 70% of the pyrolyzed material until 400 °C. It was reported [69] that primary decomposition causes 95% of total degradation. However, in the case reported here (olive stones carbonisation), only 68% of the material pyrolyzed until 400 °C, which represents the end of the primary decomposition stage. After 400 °C aromatization (secondary decomposition) reactions started [69].

3.2.7. Development of the functional groups (IR spectra)

IR results for the partially pyrolyzed OS samples are presented in Table 3. The results show that at 400 °C and above, many groups (aliphatic, alcoholic, monoaromatic, aldehyde, dien, etheric groups) have partially or completely disappeared. The mass loss between 600 and 700 °C and between 700 and 850 °C is nearly the same, which means that the carbonisation practically stopped at 600 °C, i.e. almost 96% of mass was carbonised relative to carb850 at this temperature. Bansal et al. [70] reported that carbonisation should be up to 850 °C, but did not specify the temperature in which carbonisation is complete. The data obtained here for olive stones supports this view. However, the temperature of complete carbonisation depends on the raw material and carbonisation conditions.

Cellulose degradation usually starts at 200 °C by losing adsorbed water and water produced from β-elimination of the cellulose hydroxyl groups [66]. This is revealed by a severe reduction in the O–H stretching peak. At higher temperatures, cellulose started to de-polymerize as revealed by disappearance of etheric group peaks at ~1245, 1161 and 1048 cm^{-1}. Later on, random bond breaks down of the decomposition products will produce low molar mass compounds. At 400–450 °C, aromatization started until 850 °C. Hemicellulose decomposition-depolymerization [66] took place at 220–320 °C into monomeric units then into volatiles. Lignin decomposition [66] cause the formation of large hydrocarbon molecules (tar) and then cracking and polymerisation took place. The band appeared at 1618-1623 cm^{-1} (due to symmetrical conjugated diene) at 250 °C may support this hypothesis.

3.3. The use of partially pyrolyzed OS for 2-CP removal from water

3.3.1. Adsorption of 2-CP on partially pyrolyzed OS at pH 7: Effect of pyrolysis temperature

Adsorption of 2-CP (using 40 mg L^{-1} solutions) on carb110, carb250, carb400, carb600, carb850 and carb850-activated at pH 7 was conducted. 2-CP was selected as a model chlorophenol in the present study because it has wide industrial uses and it has reasonable solubility in water. The q_e values are shown in Fig. 4A, where q_e value indicated the relative tendency (affinity) of 2-CP towards the adsorbent surface. The q_e values increased with increasing pyrolysis temperature. This may be attributed to the increase of the surface basicity (section 3.2.2) and porosity (see section 3.2.4) where both properties increased with the pyrolysis temperature. Of course both properties play a role in the phenols adsorption process. The pK_a value of 2-CP is 8.5. So that, at pH 7 the predominant species form of the phenols was the neutral form and thus the basic groups in the adsorbent surface seemed to interact with the phenol. It was reported that acidic groups potentially

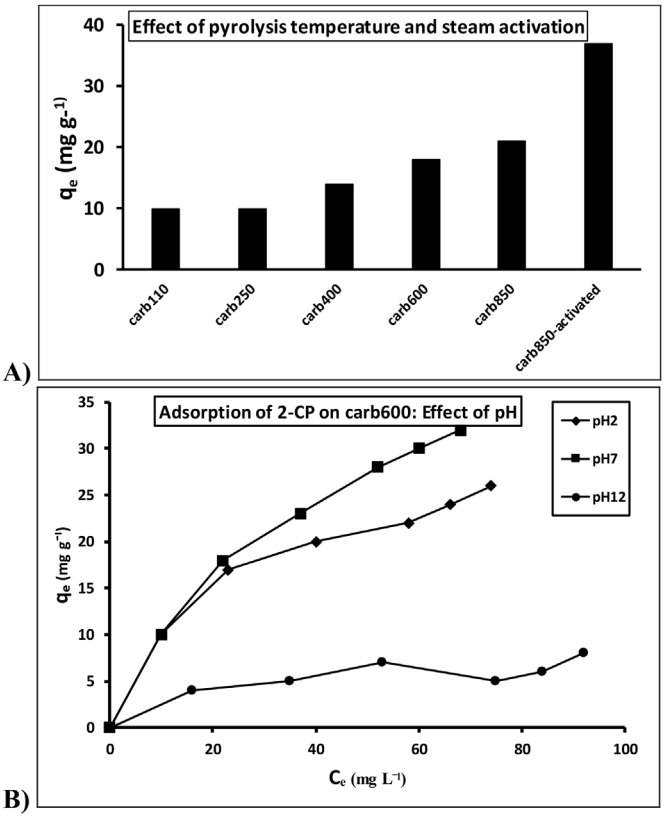

Fig. 4. A) Adsorption of 2-CP (C_o = 40 mg L^{-1}) onto various partially pyrolyzed OS at pH7: Effect of pyrolysis temperature and steam activation, B) Adsorption of 2-CP onto carb600: adsorption isotherms and effect of pH.

Table 5
Langmuir adsorption parameters of 2-CP onto carb600 at various pH values.

	X_m (mg g^{-1})	K_L	r^2
pH **2**	27.5	0.09	0.958
pH **7**	34.1	0.04	0.910
pH **12**	6.9	0.13	0.8757

inhibit the adsorption ability of carbon to adsorb phenolic compounds [44]. This was indicated by the increase in 2-CP removal with increasing pyrolysis temperature, in which the surface oxides were removed. The removal of acidic oxides on the adsorbent surface would increase the physisorption and surface polymerisation of the chlorophenols and thus increases adsorption [44].

3.3.1.1. Comparison with steam activated sorbent. A sample of carb850 was activated by steam as described in a previous work [44]. This sample was labelled carb850-activated. There was a clear difference between the adsorption efficiency of carb850-activated relative to the non-activated sorbents (carb600 and carb850); indeed, carb850-activated exhibited double q_e value relative to the non-activated sorbent carb600. The adsorbent carb850 exhibited only ~13% more sorption capacity than the sorbent carb600. So that carb600 was selected for the next step.

3.3.2. Adsorption isotherm of 2-CP on carb600 at pH 7: Effect of pH

Due to its lower energy consumption relative to carb850 and carb850-activated, carb600 was selected for drawing adsorption isotherm at various pH values. The adsorption isotherms of 2-CP on carb600 at various pH values (2, 7 and 12) is shown in Fig. 4.B, while adsorption constants of Langmuir model are shown in Table 5. The isotherms were found to follow the Langmuir model at all pH values as indicated by r^2 values. The monolayer capacity was in the following order: pH7 > pH2 > pH12.

It is well-known that surface functional groups take different forms in different media. The nature of phenols and the chemistry of the surface sites are affected by pH. All functional groups of the carbon surface are protonated at pH 2 and pH 7; but are almost deprotonated at pH > 12. The proposed structures of the functional groups on the carbon surface are shown below [71]:

In acidic medium	Carbon surface	In basic medium
Ar_π-H_3O^+	Ar_π	Ar_π
ArO^+	ArO	ArO
ArOH	ArOH	ArO^-

pKa is a measure of acidity of the compound, which is due to compound dissociation in aqueous medium. At pH > pK_a, phenolate ion concentration increased while at pH < pK_a the protonated phenol form was predominant. So that at pH 7, the neutral phenols were predominant in which they interact strongly with the neutral basic surface (π- π interaction). On the other hand, at pH 12 the negatively charged phenolate ion was predominant while the surface was either negatively charged or neutral; this situation was not ideal for phenolate adsorption due to high competition with high hydroxyl ion concentration in solution. At pH 2, the surface was positively charged or neutral and phenols were neutral; this situation was also not favoured for phenols adsorption due to strong competition with high hydronium ion concentration.

Adsorption capacity at pH7 was higher than that at pH2. At pH2, 2-CP was in non-ionic form, while surface groups were either neutral or positively charged. The interaction between carbon surface and 2-CP was weak and can be attributed to dispersion effect. This weak interaction caused co-adsorption of water. Some of the molecules interacted via hydrogen bonds formed between the protonated surface functional groups along the edge of graphitic layers and the phenolic OH groups, which might have reduced availability of graphitic region.

The fundamental interaction between carbon surface and phenols was either π-π interactions or electrostatic attraction/repulsion (if ions are present). Interaction between surface and water molecules cannot be excluded as well, and their competitive adsorption results in the depletion of the phenols adsorbed.

3.4. The optimum uptake method of 2-chlorophenol from water

25 mg of carb600 was added to a 25 mL solution containing 2-chlorophenol and the mixture was adjusted to pH 7 and shaken overnight.

3.4.1. Application on real water sample, selectivity and adsorbent re-usability

To ensure the applicability of the optimum method for environmental use, the optimum method was applied on a tap water sample (obtained from our lab) which was spiked with 40 mg 2-CP L^{-1}. The tap water sample contained 105 mg Na L^{-1}, 42 mg Ca L^{-1}, 17 mg K L^{-1}. It was found that ~70% of the adsorption efficiency was reserved (i.e. q_e was reduced by 30%). It was clear that the presence of sodium, potassium and calcium ions minor affected the selectivity of the adsorbent towards 2-CP. Re-using the adsorbent for three cycles reduced the adsorbent efficiency by 10%, which indicated that the adsorbent was re-uasble and cost-effective. The adsorbent was regenerated by washing with 5 mL ethanol each time.

4. Conclusions and recommendations

The present work presents a useful method for pollutant removal from water using partially-pyrolyzed-non-activated OS sorbent. Understanding the performance of this type of sorbents requires studying partial-stepwise pyrolysis of ground OS at various temperatures to provide information regarding mass loss during carbonisation, changes in elemental composition, crystal phases, and surface functionality and surface morphology. This may lead to a better control of the properties of the carbon produced from this source. These properties may be of both scientific and economic importance.

Olive stones did not initially show any π basicity, which then appeared gradually with increasing temperature. Acidic groups disappeared totally at 500 °C. The adsorption ability of pyrolyzed OS towards 2-CP increased with increasing pyrolysis temperature, which was due to the increase of basic groups upon pyrolysis. Indeed, the results indicated that not only non-activated carb600 could be useful for removal of phenols, but also that the lower-temperature pyrolyzed OS sorbents had poorer, but potentially useable, adsorption capabilities which would need to be balanced against lower energy demands of production depending on circumstances.

TGA showed that the major mass loss was due to primary decomposition of olive stones, which occurs between 250 and 400 °C and this constituted around 68% of the total mass lost. At 600 °C, mass loss apparently stopped. This may suggest that in any future commercial exploitation of this process, carbonisation temperature may be carried out at 600 °C, rather than 850 °C. However, MB adsorption data, BET and SEM showed a

heterogeneous surface and undeveloped porosity to be dominant before 850 °C. Thus we should not ignore the critical role of the reactions taking place between 600 and 850 °C, although no IR data supported this issue. Indeed, the major porosity development occurs upon activation (activation was applied in the present work for comparative purpose only). If pyrolysis is carried out at 600 °C, rather than 850 °C, then this may potentially save energy and produce more adsorbent mass in the carbonisation process, but other factors such as the quality of any gaseous or liquid by-products may need to be considered before such a decision is reached. Clearly further product development and process scale-up is required but partial pyrolysis of olive stones seems to offer a potential method of converting a waste material into a useful product. Not only could low-temperature pyrolysis and omission of the activation step save energy, but also produce larger mass of adsorbent capable of pollutants removal (such as 2-CP) from water.

Declaration of competing interest

The authors of the present manuscript have no conflict of interest to declare.

Appendix A. Supplementary data

Supplementary data to this article can be found online at https://doi.org/10.1016/j.emcon.2023.100209.

References

[1] T.R. Brazil, M. Gonçalves, M.S.O. Junior, M.C. Rezende, A statistical approach to optimize the activated carbon production from Kraft lignin based on conventional and microwave processes, Microporous Mesoporous Mater. 308 (2020), 110485.

[2] J. Ouyang, L. Zhou, Z. Liu, J.Y.Y. Heng, W. Chen, Biomass-derived activated carbons for the removal of pharmaceutical mircopollutants from wastewater: a review, Separ. Purif. Technol. 253 (2020), 117536.

[3] F. Parvin, N.M. Niloy, M.M. Haque, S.M. Tareq, Chapter 7 - activated carbon as potential material for heavy metals removal from wastewater, in: Akil Ahmad, Rajeev Kumar, Mohammad Jawaid, Emerging Techniques for Treatment of Toxic Metals from Wastewater, Elsevier, 2023, pp. 117–130, 2023.

[4] B.M. Esteves, S. Morales-Torres, F.J. Maldonado-Hódar, L.M. Madeira, Sustainable iron-olive stone-based catalysts for Fenton-like olive mill wastewater treatment: development and performance assessment in continuous fixed-bed reactor operation, Chem. Eng. J. 435 (2022), 134809.

[5] B.M. Esteves, S. Morales-Torres, L.M. Madeira, F.J. Maldonado-Hódar, Specific adsorbents for the treatment of OMW phenolic compounds by activation of bio-residues from the olive oil industry, J. Environ. Manag. 306 (2022), 114490.

[6] M. Corral-Bobadilla, R. Lostado-Lorza, F. Somovilla-Gómez, R. Escribano-García, Effective use of activated carbon from olive stone waste in the biosorption removal of Fe(III) ions from aqueous solutions, J. Clean. Prod. 294 (2021), 126332.

[7] M. Al-Ghouti, A.O. Sweleh, Optimizing textile dye removal by activated carbon prepared from olive stones, Environ. Technol. Innovat. 16 (2019), 100488.

[8] R. Ahmed, G. Liu, B. Yousaf, Q. Abbas, H. Ullah, Muhammad Ubaid Ali, Recent advances in carbon-based renewable adsorbent for selective carbon dioxide capture and separation-A review, J. Clean. Prod. 242 (2020), 118409.

[9] R. Mustafa, E. Asmatulu, Preparation of activated carbon using fruit, paper and clothing wastes for wastewater treatment, J. Water Proc. Eng. 35 (2020), 101239.

[10] Z. Rouzitalab, D.M. Maklavany, S. Jafarinejad, A. Rashidi, Lignocellulose-based adsorbents: a spotlight review of the effective parameters on carbon dioxide capture process, Chemosphere 246 (2020), 125756.

[11] Md M. Hasan, M.A. Shenashen, Md N. Hasan, H. Znad, Md S. Salman, Md R. Awual, Natural biodegradable polymeric bioadsorbents for efficient cationic dye encapsulation from wastewater, J. Mol. Liq. 323 (2021), 114587.

[12] Md B. Yeamin, MdM. Islam, A. Chowdhury, Md R. Awual, Efficient encapsulation of toxic dyes from wastewater using several biodegradable natural polymers and their composites, J. Clean. Prod. 291 (2021), 125920.

[13] S. Khandaker, M.F. Chowdhury, Md R. Awual, A. Islam, T. Kuba, Efficient cesium encapsulation from contaminated water by cellulosic biomass based activated wood charcoal, Chemosphere 262 (2021), 127801.

[14] H. Znad, H. Al-Mohammedawi, Md R. Awual, Integrated pre-treatment stage of biosorbent – sonication for mixed brewery and restaurant effluents to enhance the photo-fermentative hydrogen production, Biomass Bioenergy 144 (2021), 105899.

[15] S. Khandaker, Md T. Hossain, P.K. Saha, U. Rayhan, A. Islam, T.R. Choudhury, Md R. Awual, Functionalized layered double hydroxides composite bio-adsorbent for efficient copper(II) ion encapsulation from wastewater, J. Environ. Manag. 300 (2021), 113782.

[16] P. Miretzky, A. Cirelli, Cr(VI) and Cr(III) removal from aqueous solution by raw and modified lignocellulosic materials: a review, J. Hazard Mater. 180 (2010) 1–19.

[17] A. Agarwal, U. Upadhyay, I. Sreedhar, S.A. Singh, C.M. Patel, A review on valorization of biomass in heavy metal removal from wastewater, J. Water Proc. Eng. 38 (2020), 101602.

[18] N.H. Solangi, J. Kumar, S.A. Mazari, S. Ahmed, N. Fatima, N.M. Mubarak, Development of fruit waste derived bio-adsorbents for wastewater treatment: a review, J. Hazard Mater. 416 (2021), 125848.

[19] A.H. El-Sheikh, H.S. Alshamaly, Cadmium removal from organic acid-bearing soil-washing water by magnetic biosorption: effect of various factors and adsorption isothermal study, J. Environ. Chem. Eng. 8 (2020), 104188.

[20] M.E. Abdel-Raouf, Chapter 5 - fruit stones as green materials for wastewater remediation, in: s), A. Ahmad, R. Kumar, M. Jawaid (Eds.), Emerging Techniques for Treatment of Toxic Metals from Wastewater, Elsevier, 2023, pp. 83–101, 2023.

[21] W. Tariq, C. Arslan, N. Tayyab, H. Rashid, A. Nasir, Chapter 9 - application of agro-based adsorbent for removal of heavy metals, in: s), A. Ahmad, R. Kumar, M. Jawaid (Eds.), Emerging Techniques for Treatment of Toxic Metals from Wastewater, Elsevier, 2023, pp. 157–182, 2023.

[22] M. Bashir, S. Tyagi, A.P. Annachhatre, Adsorption of copper from aqueous solution onto agricultural Adsorbents: kinetics and isotherm studies, Mater. Today Proc. 28 (2020) 1833–1840.

[23] C.O. Thompson, A.O. Ndukwe, C.O. Asadu, Application of activated biomass waste as an adsorbent for the removal of lead (II) ion from wastewater, Emerg. Contaminant. 6 (2020) 259–267.

[24] H.K. Okoro, S. Pandey, C.O. Ogunkunle, C.J. Ngila, C. Zvinowanda, I. Jimoh, I.A. Lawal, M.M. Orosun, A.G. Adeniyi, Nanomaterial-based biosorbents: adsorbent for efficient removal of selected organic pollutants from industrial wastewater, Emerg. Contaminant. 8 (2022) 46–58.

[25] M. Contreras, I. Romero, M. Moya, E. Castro, Olive-derived biomass as a renewable source of value-added products, Process Biochem. 97 (2020) 43–56.

[26] K. Kiełbasa, S. Bayar, E.A. Varol, J. Sreńscek-Nazzal, M. Bosacka, B. Michalkiewicz, Thermochemical conversion of lignocellulosic biomass -olive pomace - into activated biocarbon for CO2 adsorption, Ind. Crop. Prod. 187 (2022), 115416.

[27] A.H. El-Sheikh, J.A. Sweileh, M.I. Saleh, Partially-pyrolyzed olive pomace sorbent of high permeability for preconcentration of metals from environmental waters, J. Hazard Mater. 169 (2009) 58–64.

[28] A. Agarwal, U. Upadhyay, I. Sreedhar, K.L. Anitha, Simulation studies of Cu(II) removal from aqueous solution using olive stone, Clean. Mater. 5 (2022), 100128.

[29] A.H. El-Sheikh, Partial pyrolysis of olive wood to improve its sorption of chlorophenols and nitrophenols, Int. J. Environ. Sci. Technol. 11 (2014) 1459–1472.

[30] M.A. Khan, A.A. Alqadami, S.M. Wabaidur, M.R. Siddiqui, B. Jeon, S.A. Alshareef, Z.A. Alothman, A.E. Hamedelniel, Oil industry waste based non-magnetic and magnetic hydrochar to sequester potentially toxic post-transition metal ions from water, J. Hazard Mater. 400 (2020), 123247.

[31] A.H. El-Sheikh, I.I. Fasfous, R.M. Al-Salamin, A.P. Newman, Immobilization of citric acid and magnetite on sawdust for competitive adsorption and extraction of metal ions from environmental waters, J. Environ. Chem. Eng. 6 (2018) 5186–5195.

[32] L. Capobianco, F.D. Caprio, P. Altimari, M.L. Astolfi, F. Pagnanelli, Production of an iron-coated adsorbent for arsenic removal by hydrothermal carbonization of olive pomace: effect of the feedwater pH, J. Environ. Manag. 273 (2020), 111164.

[33] A.H. El-Sheikh, A.M. Shudayfat, I.I. Fasfous, Preparation of magnetic bio-sorbents based on cypress wood that was pretreated by heating or TiO_2 deposition, Ind. Crop. Prod. 129 (2019) 105–113.

[34] A.H. El-Sheikh, A.M. Alzawahreh, J.A. Sweileh, Preparation of an efficient sorbent by washing then pyrolysis of olive wood for simultaneous solid phase extraction of chloro-phenols and nitro-phenols from water, Talanta 85 (2011) 1034, 1042.

[35] B. Esteves, H. Pereira, Wood modification by heat treatment: a review, Bio-resources 4 (2009) 370–404.

[36] K. Yuney, A.A. Oladipo, M. Gazi, D.Z. Younis, CuO coated olive cake nano-composites for rapid phenol removal and effective discoloration of high strength olive mill wastewater, Chemosphere 253 (2020), 126703.

[37] M. Rodriguez-Valero, M. Martines-Escandell, M. Molina-Sabio, F. Rodriguez-Reinoso, CO2 activation of olive stones carbonized under pressure, Carbon 39 (2001) 320–323.

[38] P. Galiatsatou, V. Metaxas, V. Kasseloui-Rigopoulou, Mesoporous activated carbon from agricultural byproducts, Mikrochim. Acta 136 (2001) 147–152.

[39] C. Mangwandi, T.A. Kurniawan, A.B. Albadarin, Comparative biosorption of chromium (VI) using chemically modified date pits (CM-DP) and olive stone (CM-OS): kinetics, isotherms and influence of co-existing ions, Chem. Eng. Res. Des. 156 (2020) 251–262.

[40] M. Imran-Shaukat, R. Wahi, Z. Ngaini, The application of agricultural wastes for heavy metals adsorption: a meta-analysis of recent studies, Bioresource

Technol. Rep. 17 (2022), 100902.
[41] H. Nassar, A. Zyoud, A. El-Hamouz, R. Tanbour, N. Halayqa, H.S. Hilal, Aqueous nitrate ion adsorption/desorption by olive solid waste-based carbon activated using ZnCl2, Sustain. Chem. Pharm. 18 (2020), 100335.
[42] R. Estevez, L. Aguado-Deblas, V. Montes, A. Caballero, F.M. Bautista, Sulfonated carbons from olive stones as catalysts in the microwave-assisted etherification of glycerol with tert-butyl alcohol, Mol. Catal. 488 (2020), 110921.
[43] D. Pandey, A. Daverey, K. Arunachalam, Biochar: production, properties and emerging role as a support for enzyme immobilization, J. Clean. Prod. 255 (2020), 120267.
[44] A.H. El-Sheikh, A.P. Newman, H.K. Al-Daffaee, S. Phull, D. Lynch, The use of activated carbon of basic nature for treatment of 2-chlorophenol, Adsorpt. Sci. Technol. 22 (2004) 451–465.
[45] P. Zong, Y. Cheng, S. Wang, L. Wang, Simultaneous removal of Cd (II) and phenol pollution through magnetic graphene oxide nanocomposites coated polyaniline using low temperature plasma technique, Int. J. Hydrogen Energy 45 (2020) 20106–20119.
[46] S.A. Hosseini, M. Davodian, A.R. Abbasian, Remediation of phenol and phenolic derivatives by catalytic wet peroxide oxidation over Co-Ni layered double nano hydroxides, J. Taiwan Inst. Chem. Eng. 75 (2017) 97–104.
[47] A.H. El-Sheikh, M.K. Al-Jafari, J.A. Sweileh, Solid phase extraction and uptake properties of multi-walled carbon nanotubes of different dimensions towards some nitro-phenols and chloro-phenols from water, Int. J. Environ. Anal. Chem. 92 (2012) 190–209.
[48] A.H. Mady, M.L. Baynosa, D. Tuma, J.J. Shim, Heterogeneous activation of peroxymonosulfate by a novel magnetic 3D γ-MnO2@ ZnFe2O4/rGO nanohybrid as a robust catalyst for phenol degradation, Appl. Catal. B Environ. 244 (2019) 946–956.
[49] J. Michałowicz, W. Duda, Phenols–Sources and toxicity, Pol. J. Environ. Stud. 16 (2007) 347–362.
[50] K.M. Basha, A. Rajendran, V. Thangavelu, Recent advances in the biodegradation of phenol: a review, Asian J. Experimen. Biol. Sci. 1 (2010) 219–234.
[51] E. Sjostrom, Wood Chemistry: Fundamentals and Applications, Academic Press, New York, 1981.
[52] H.P. Boehm, Surface oxides on carbon and their analysis: a critical assessment, Carbon 40 (2002) 145–149.
[53] Mu Naushad, , Ayoub Abdullah Alqadami, A. Abdullah, Al-Kahtani, Tansir Ahamad, Md. Rabiul Awual, etiana Tatarchuk, Adsorption of textile dye using para-aminobenzoic acid modified activated carbon: kinetic and equilibrium studies, J. Mol. Liq. 296 (2019), 112075.
[54] Md Nazmul Hasan, M.A. Shenashen, Md Munjur Hasan, Hussein Znad, Md Rabiul Awual, Assessing of cesium removal from wastewater using functionalized wood cellulosic adsorbent, Chemosphere 270 (2021), 128668.
[55] M.R. Awual, An efficient composite material for selective lead(II) monitoring and removal from wastewater, J. Environ. Chem. Eng. 7 (2019), 103087.
[56] M.R. Awual, Mesoporous composite material for efficient lead(II) detection and removal from aqueous media, J. Environ. Chem. Eng. 7 (2019), 103124.
[57] M.R. Awual, A facile composite material for enhanced cadmium(II) ion capturing from wastewater, J. Environ. Chem. Eng. 7 (2019), 103378.
[58] Amjad H. El-Sheikh, Jamal A. Sweileh, Sorption of trace metals on fish scales and application for lead and cadmium pre-concentration with flame atomic absorption determination, Jordan J. Chem. 3 (2008) 87–97.
[59] Amjad H. El-Sheikh, Jamal A. Sweileh, Recent applications of carbon nanotubes in solid phase extraction and preconcentration: a review, Jordan J. Chem. 6 (2011) 1–16.
[60] Amjad H. El-Sheikh, Jamal A. Sweileh, A rapid and simple microwave-assisted digestion procedure for spectrophotometric determination of titanium dioxide photocatalyst on activated carbon, Talanta 71 (2007) 1867–1872.
[61] Alireza Fathollahi, Stephen J. Coupe, H. Amjad, El-Sheikh, Ernest O. Nnadi, Cu(II) biosorption by living biofilms: isothermal4, chemical, physical and biological evaluation, J. Environ. Manag. 282 (2021), 111950.
[62] Alireza Fathollahi, Steve J. Coupe, H. Amjad, El-Sheikh, L.A. Sañudo-Fontaneda, The biosorption of mercury by permeable pavement biofilms in stormwater attenuation, Sci. Total Environ. 741C (2020), 140411.
[63] Jafar I. Abdelghani, Rami S. Freihat, Amjad H. El-Sheikh, Magnetic solid phase extraction of phthalate products from bottled, injectable and tap waters using graphene oxide: effect of oxidation method of graphene, J. Environ. Chem. Eng. 8 (2020), 103527.
[64] E. Iniesta, F. Sanchez, A. Garcia, A. Marcilla, Yields and CO_2 reactivity of chars from almond shells obtained by a two heating step carbonisation process. Effect of different chemical pre-treatment and ash content, J. Anal. Appl. Pyrol. 58 (2001) 983–994.
[65] R.P. Overend, E. Chornet, in: 4th Conference on Biomass: A Growth Opportunity in Green Energy and Value-Added Products, Pergamon-Elsevier Science, Oxford, 1999.
[66] A.V. Bridgwater, Thermogravimetric analysis of the components of biomass, in: Advances in Thermochemical Biomass Conversion, Blackie Academic and Professional, London, 1994.
[67] A. Marcilla, M. Asenio, I. Martingullon, Influence of carbonisation heating rate in the physical properties of activated carbons, First Europ. Conf. Young Res. Chem. Eng. 1–2 (1995) 508–510, 5-6 Jan 1995, Edinburg, Scotland.
[68] J.M. Nazzal, Influence of heating rate on pyrolysis of Jordan oil shale, J. Anal. Appl. Pyrol. 62 (2002) 225–238.
[69] M. Hajaligol, B. Waymack, D. Kellogg, Pyrolysis behaviour and kinetics of biomass derived materials, J. Anal. Appl. Pyrol. 62 (2002) 331–349.
[70] R. Bansal, J. Donnet, F. Stoeckli, Active Carbon, Marcel Dekker, New York, 1998.
[71] K. Laszlo, Adsorption from aqueous phenol and 2,3,4-trichlorophenol solutions on nanoporous carbon prepared from poly (ethylene terephtalate), Adsorp. Nanostruc. 117 (2001) 5–12.